Original Article

MOLECULAR METABOLISM

Macrophages sensing oxidized DAMPs reprogram their metabolism to support redox homeostasis and inflammation through a TLR2-Syk-ceramide dependent mechanism

Vlad Serbulea [1], Clint M. Upchurch [1], Katelyn W. Ahern [1,2], Gael Bories [1], Paxton Voigt [1], Dory E. DeWeese [1], Akshaya K. Meher [1], Thurl E. Harris [1,2], Norbert Leitinger [1,2,*]

ABSTRACT

Objective: Macrophages control tissue homeostasis and inflammation by sensing and responding to environmental cues. However, the metabolic adaptation of macrophages to oxidative tissue damage and its translation into inflammatory mechanisms remains enigmatic.
Methods: Here we identify the critical regulatory pathways that are induced by endogenous oxidation-derived DAMPs (oxidized phospholipids, OxPL) *in vitro*, leading to formation of a unique redox-regulatory metabolic phenotype (Mox), which is strikingly different from conventional classical or alternative macrophage activation.
Results: Unexpectedly, metabolomic analyses demonstrated that Mox heavily rely on glucose metabolism and the pentose phosphate pathway (PPP) to support GSH production and Nrf2-dependent antioxidant gene expression. While the metabolic adaptation of macrophages to OxPL involved transient suppression of aerobic glycolysis, it also led to upregulation of inflammatory gene expression. In contrast to classically activated (M1) macrophages, Hif1α mediated expression of OxPL-induced Glut1 and VEGF but was dispensable for Il1β expression. Mechanistically, we show that OxPL suppress mitochondrial respiration via TLR2-dependent ceramide production, redirecting TCA metabolites to GSH synthesis. Finally, we identify spleen tyrosine kinase (Syk) as a critical downstream signaling mediator that translates OxPL-induced effects into ceramide production and inflammatory gene regulation.
Conclusions: Together, these data demonstrate the metabolic and bioenergetic requirements that enable macrophages to translate tissue oxidation status into either antioxidant or inflammatory responses via sensing OxPL. Targeting dysregulated redox homeostasis in macrophages could therefore lead to novel therapies to treat chronic inflammation.

Keywords Oxidized phospholipids; Spleen tyrosine kinase; Macrophages; Bioenergetics; Cellular metabolism; Redox homeostasis; Inflammation; Ceramides

1. INTRODUCTION

Macrophages have been shown to play essential roles in maintenance of tissue homeostasis as well as in regulation of induction and resolution of inflammation in response to tissue injury or infection [1,2]. The functional plasticity of macrophages has been tied to changes in their cellular metabolism [3–5]. In general, inflammation-promoting classically activated (M1) macrophages rely on aerobic glycolysis and succinate-driven Hif1α-dependent glycolytic gene expression, which is necessary for bacterial ligand-induced pro-inflammatory cytokine production [6]. On the other hand, anti-inflammatory, alternatively activated (M2) macrophages rely on oxidative phosphorylation (OXPHOS) with a possible role for fatty acid oxidation in phenotypic polarization and sustained function [7,8]. We have previously identified phenotypically polarized macrophages in atherosclerotic lesions, coined Mox, that respond to oxidized phospholipids (OxPLs) by upregulating Nrf2-dependent antioxidant enzymes [9]. However, the cellular metabolism of Mox macrophages has not been described.

OxPL have been identified as endogenous danger associated molecular patterns (DAMPs), characteristic of oxidatively damaged tissue, and they were shown to be key players in cardiovascular disease. The Copenhagen General Population Study revealed that OxPLs are risk factors for calcific aortic valve disease [10]. This study also showed a close correlation of OxPLs and lipoprotein(a), which has been previously associated with calcific aortic valve disease and atherosclerosis in humans and mice [11–13]. Chronic inflammatory diseases like atherosclerosis are macrophage-driven diseases, which may involve

[1]Department of Pharmacology, University of Virginia, Charlottesville, VA 22903, USA [2]Robert M. Berne Cardiovascular Research Center, University of Virginia, Charlottesville, VA 22903, USA

*Corresponding author. Department of Pharmacology, University of Virginia, 1340 Jefferson Park Ave, Charlottesville, VA 22903, USA. E-mail: nl2q@virginia.edu (N. Leitinger).

Received October 3, 2017 • Revision received October 28, 2017 • Accepted November 1, 2017 • Available online 7 November 2017

https://doi.org/10.1016/j.molmet.2017.11.002

the action of OxPLs, making it essential to better understand the signaling pathways that are induced by OxPLs in macrophages.

OxPAPC is a mixture of individual OxPL species derived from free radical-induced oxidation of 1-palmitoyl-2-arachidonoyl-sn-glycero-3-phosphatidylcholine (PAPC) [14–17]. In macrophages, OxPAPC has been shown to drive TLR2-dependent pro-inflammatory [18,19] and Nrf2-dependent antioxidant responses [9,20–23]. Furthermore, OxPAPC has been shown to inhibit classic LPS-driven TLR4-dependent inflammatory responses [19,24,25], but also to induce non-canonical Caspase11-driven inflammasome activation [26]. Although OxPLs induce inflammatory gene expression, they do not induce NF-κB signaling [27]. Mounting evidence suggests that spleen tyrosine kinase (Syk), a target of the drug fostamatinib [28], is downstream of TLR2 signaling induced by a variety of ligands [29–33]. Syk has been shown to play a crucial role in the action of oxidized cholesteryl esters on macrophages [34–36], and treatment with the orally available Syk inhibitor, fostamatinib, prevented atherogenesis in LDLR-receptor deficient mice fed a high-fat diet [37].

Here we show that macrophages sense OxPL to reprogram their metabolism towards a redox-regulatory phenotype accompanied by antioxidant and inflammatory gene expression, via a mechanism involving TLR2 and Syk-driven ceramide accumulation. Together, we provide a new model for macrophage adaptation to oxidative tissue damage, revealing unexpected roles of TLR2, ceramides, and Hif1a in cellular metabolic reprogramming and translation into inflammatory gene expression.

2. MATERIALS AND METHODS

2.1. Mice

C57BL/6, TLR2-KO, Hif-1α-KO, and Nrf2-KO mice were obtained from Jackson Laboratories and housed in the Pinn vivarium, at the University of Virginia, according to standard animal care and use practices dictated by the University of Virginia's Institutional Animal Care and Use Committee (IACUC).

2.2. Air oxidation of phospholipids

Chemical Reagents — 1-palmitoyl-2-arachidonoyl-3-glycero-phosphatidylcholine (PAPC), 1-palmitoyl-2-glutaryl-3-glycero-phosphatidylcholine (PGPC), and 1-palmitoyl-2-arachidonoyl-3-glycero-phosphatidylethanolamine (PAPE) were obtained from Avanti Polar Lipids, Inc. PAPC or PAPE (1 mg) were dried down in a glass tube, covered loosely with foil, and allowed to oxidized by air for five to twelve days. The oxidation status was monitored by direct injection fragmentation mass spectrometry analysis as well as liquid chromatography–mass spectrometry quantification. The final mixtures of phospholipids were referred to as OxPAPC or OxPAPE and were re-suspended in cell culture media (RPMI with 10% FBS, 2% HEPES, and 1% Antibiotic–Antimycotic) for cell treatment.

2.3. Bone marrow isolation and culture

The bone marrow from the hind legs of mice was isolated and cleared of erythrocyte progenitors using short incubation with 0.83% ammonium chloride. The bone marrow was then cultured with RPMI media, containing 10% fetal bovine serum (Atlanta Biologicals), 2% HEPES (Gibco), 1% Antibiotic–Antimycotic (Gibco), and 10% L929-conditioned media (L929 cells purchased from ATCC). The culture continued for 7 days, with media changes every 3 days, after which, the media was exchanged for one lacking the L929-conditioned media. On day 7, the bone marrow-derived macrophages (BMDMs) were gently separated from Petri dishes using 0.25% trypsin (Gibco), centrifuged, had their media refreshed, and re-plated for analysis.

2.4. Metabolomics

For each sample, the bone marrow from the hind legs of one mouse was harvested and cultured into BMDMs. These BMDMs were then treated with OxPAPC, LTA, or IL4 for 6 h to polarize them to Mox, classically activated M1, or alternatively activated M2 macrophages, respectively. Trypsin was used to dislodge the cells from their plates, and each sample was centrifuged at 600 × *g* for 5 min to pellet the cells. The supernatant was vacuumed off and the cell pellet was stored at −80 °C prior to transport to Metabolon, Inc. who performed the global metabolomic analysis.

2.5. qRT-PCR

RNA was isolated from cells using the RNEasy Mini Kit. Libraries of cDNA were produced using the iScript cDNA Synthesis Kit. Quantitative real-time PCR (qRT-PCR) was set up using 250 ng of cDNA and SensiMix SYBR & Fluorescein Kit. Primer sequences can be found in Table S2. Primers were designed with Primer Blast and validated using melt curve analysis.

2.6. Ceramide measurement by LC–MS

To measure ceramides, 200 μL of chloroform was added to 100 μL homogenate, and the homogenate was incubated overnight at 48 °C. After cooling to room temperature, 20 μL of 1 M KOH in methanol was added, and the samples were incubated at 37 °C for 2 h. Lipids were neutralized with 5 μL of glacial acetic acid. 1.5 mL of HPLC-grade chloroform and 2 mL of H_2O (Fisher) were added to each sample, vortexed, and centrifuged at 600 × *g* for 10 min to separate the organic and aqueous phases. The organic phase was dried under argon prior to resuspension in mobile phase solvent containing 97% acetonitrile, 2% methanol, and 1% formic acid (v/v/v) supplemented with 5 mM ammonium formate. Using a Sciex 4000 QTrap, a triple quadrupole mass spectrometer, coupled to a Shimadzu LC-20AD LC system equipped with a Supelcosil LC-NH2 HPLC column (3 μm, 50 cm × 2.1 mm) samples were subjected to normal phase LC–MS/MS. We employed a multiple reaction monitoring scheme for naturally occurring species of saturated and unsaturated ceramides, ranging from Cer16:0 to Cer24:2. Data were acquired as previously described, and quantification was carried out by integrating peak areas for each individual analyte using Analyst 1.5.1 software. Recovery was assessed using internal standards, and values were normalized to protein content measured by a Bradford Assay.

2.7. Mitochondrial and glycolytic stress tests

Cells were seeded into a Seahorse 24-well tissue culture plate (Agilent Technologies, Santa Clara, CA). The cells adhered for 1–2 h prior to treatment. For assessing respiratory capacity, cells were subjected to a mitochondrial stress test as established previously [38], briefly described here. At the beginning of the assay, the media was changed to DMEM with pyruvate (Thermo-Fisher Cat#: 12800017, pH = 7.35 at 37 °C), and cells were allowed to equilibrate for 30 min. Oxygen consumption rate (OCR) was measured using a Seahorse XF24 Flux Analyzer (Agilent Technologies, Santa Clara, CA). After three basal OCR measurements, compounds to modulate cellular respiratory function [1 μM Oligomycin (Sigma–Aldrich); 2 μM BAM15 (Cayman Chemical Company); 1 μM Antimycin A & 100 nM Rotenone (Sigma–Aldrich)] were injected into the plate after every three measurements, and OCR was measured using four-minute measurement periods. Basal respiration was calculated by subtracting the average of the post-Antimycin A and Rotenone measurements from the average of the first three measurements. Maximum respiratory capacity was calculated by subtracting the average of the post-Antimycin A & Rotenone

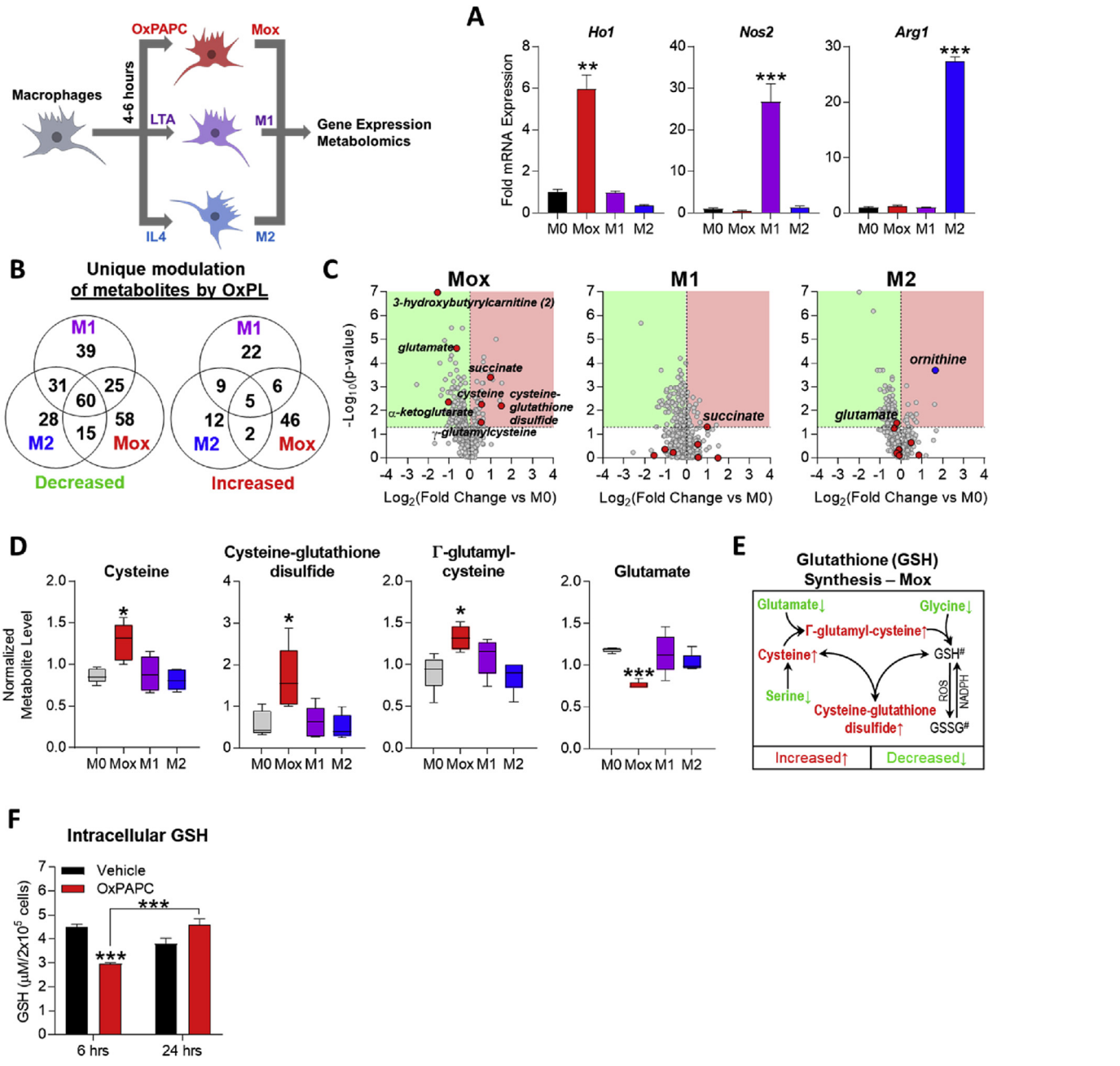

Figure 1: OxPLs induce a metabolic shift to glutathione synthesis in macrophages. A. mRNA expression by qPCR measured in BMDMs treated with 1 μg/mL LTA (M1), 10 ng/mL IL4 (M2), or 10 μg/mL OxPAPC (Mox) for 4 h. Genes measured are *Nos2* (iNOS; M1 marker), *Arg1* (M2 marker), and *Ho1* (Mox marker) ($n \geq 3$). **B.** Metabolomics was performed on bone marrow-derived macrophages (BMDMs; harvested and cultured from C57BL/6 mouse hind legs) after 6 h treatment with M0 (vehicle, RPMI media), M1 (1 μg/mL LTA), M2 (10 ng/mL IL4), and Mox (10 μg/mL OxPAPC) stimuli ($n = 5$). Of a total of 512 metabolites of known identity, following normalization to protein concentration by Bradford assay, Welch's two-sample t-test was used to identify metabolites that differed significantly between experimental groups. A summary of the numbers of metabolites that achieved statistical significance (Welch's 2-sided t-test, $p \leq 0.05$) either uniquely per individual treatment or commonly between treatments, represented in a Venn diagram ($n = 5$). **C.** Volcano plots produced using data from metabolomics of polarized BMDMs (see A) highlighting significantly ($p \leq 0.05$) increased (red) or decreased (green) metabolites per group. Metabolites related to energy metabolism and redox homeostasis significantly changed in Mox (OxPAPC-treated) BMDMs are highlighted as red circles in each panel. Ornithine is highlighted in the M2 (IL4-treated) BMDMs as a positive control. **D.** Quantification of individual metabolites involved in the glutathione synthesis pathway in BMDMs represented by box and whisker plots. The highest and lowest bars represent the maximum distribution, while the upper, middle, and lower lines of the box represent the first quartile, median, and third quartile, respectively ($n = 5$). **E.** Glutathione synthesis pathway in Mox BMDMs (10 μg/mL OxPAPC, 6 h). #GSH (reduced glutathione) and GSSG (oxidized glutathione) levels were not measured. **F.** Intracellular reduced glutathione (GSH) levels in BMDMs treated for 6 or 24 h with vehicle (RPMI media) or 10 μg/mL OxPAPC, measured using the GSH/GSSG Ratio Detection Assay Kit (Abcam; ab138881) ($n = 4$). Data are expressed as mean ± SEM. Biological replicates indicated by (n). Statistical significance calculated by Welch's 2-sided t-test (*$p \leq 0.05$; **$p < 0.01$; ***$p < 0.001$).

measurements from the average of the post-BAM15 measurements. The reserve capacity was calculated by subtracting the average of the basal measurements from the average of the post-BAM15 measurements. For assessing glycolytic capacity, cells were subjected to a glycolytic stress test, briefly described here. For this test, extracellular acidification rate (ECAR), representing the secretion of lactate, was measured using a Seahorse XF24 Flux Analyzer. Cells were seeded into a Seahorse 24-well tissue culture plate. At the beginning of the assay, the media was changed to unbuffered, glucose-free DMEM (Sigma–Aldrich Cat#: D5030, pH = 7.35 at 37 °C), supplemented with 143 mM NaCl and 2 mM Glutamine. After three basal ECAR measurements, compounds to modulate glycolysis (20 mM Glucose; 1 μM Oligomycin; 80 mM 2-Deoxyglucose) (Sigma) were injected after every four measurements, and ECAR was measured using three-minute measurement periods. Basal glycolysis was calculated by subtracting the average of the post-2-Deoxyglucose measurements from the average of the post-Glucose measurements. Maximum glycolytic capacity was calculated by subtracting the average of the post-2-Deoxyglucose measurements from the average of the post-Oligomycin measurements. The glycolytic reserve capacity was calculated by subtracting the average of the post-Oligomycin measurements from the average of the post-Glucose measurements.

3. RESULTS

3.1. OxPLs induce a metabolic shift to glutathione (GSH) synthesis in macrophages

Recently, the metabolomic profiles of M1 and M2 macrophages have been described [8], demonstrating a shift to a highly glycolytic metabolism in M1 [6,39] and a dependence on oxidative phosphorylation in M2 macrophages [7]. To investigate the cellular metabolism of Mox macrophages, we performed metabolomic analyses (Metabolon, Inc.) on bone marrow-derived macrophages (BMDMs) that had been treated with either vehicle, OxPAPC, the TLR2 agonist lipoteichoic acid (LTA), or interleukin-4 (IL4) for 4 h, to induce M0, Mox, M1, or M2 phenotypic polarization, respectively (Figure 1A) [9]. Comparison of the phenotypes revealed that Mox macrophages displayed a metabolomic profile strikingly different from M1 or M2 macrophages, characterized by 104 uniquely regulated metabolites (Figure 1B). Volcano plots illustrated that most of the metabolites that were uniquely and most significantly changed in Mox macrophages belonged to energy metabolism and antioxidant production pathways (Figure 1C) and included cysteine, cysteine-glutathione disulfide, and γ-glutamyl-cysteine (Figure 1D), essential components of the glutathione synthesis pathway. Furthermore, only in Mox macrophages were glutamate levels significantly decreased, consistent with its use for glutathione synthesis (Figure 1D). Together, these data demonstrate that the glutathione synthesis pathway is specifically upregulated in Mox (Figure 1E) but not in M1 or M2 macrophages (Figure S1A).

In order to alleviate oxidative stress, initially depleted glutathione needs to be replenished over time to restore redox homeostasis, as has been shown in macrophages treated with oxidized LDL [40]. We found that treatment of macrophages with OxPAPC significantly decreases reduced glutathione (GSH) levels after 6 h (Figure 1F), but after 24-h GSH levels returned to normal, indicative of *de novo* GSH production (Figure 1F). On the other hand, in LTA-treated macrophages GSH levels remained unchanged after 6 and 24 h (Figure S1B).

Taken together, these data demonstrate that macrophages uniquely respond to phospholipid oxidation products by initially channeling their metabolism to adopt a redox-regulating phenotype.

3.2. OxPL-treated macrophages induce the pentose phosphate pathway while relying on glucose metabolism for antioxidant gene expression

M1 macrophages utilize glucose and M2 macrophages use fatty acids for energy production [6,7]; however, the fuel source for Mox macrophages is not known. Metabolomic analysis demonstrated that glucose levels significantly increased in OxPAPC-treated macrophages (Figure 2A), suggesting that Mox macrophages utilize glucose as fuel for cellular functions. Indeed, treatment of BMDMs with OxPAPC for 6 h resulted in a concentration-dependent increase of intracellular glucose levels, comparable to effects of the TLR2 ligand LTA or insulin (Figure 2B). Furthermore, OxPAPC induced expression of *Glut1* mRNA in BMDMs in a concentration- and time-dependent manner (Figure 2C). Next, we investigated whether glucose metabolism is required for the OxPAPC-induced expression of Nrf2-dependent enzymes. We found that pre-treatment of BMDMs with 10 mM 2-deoxyglucose (2-DG), a competitive inhibitor of hexokinase (given at half the concentration of glucose in the culture medium), blocked OxPAPC-induced *Gclm*, *Ho1*, *Srxn1*, and *Txnrd1* expression (Figure 2D). Furthermore, we found that the OxPAPC and 2-DG co-treated macrophages did not recover GSH levels after 24 h (Figure S1C), although GSH levels were still significantly higher than in macrophages treated with 2-DG alone. These data show that glucose metabolism plays an essential role in glutathione synthesis in Mox macrophages.

Many of the Nrf2-dependent enzymes, such as those involved in GSH synthesis, require NADPH as a reducing equivalent [41–45], which is primarily produced by the pentose phosphate pathway (PPP) [46,47]. We found that 6-h treatment of macrophages with OxPAPC significantly depleted NADPH (Figure 2E), and 6 and 24-h treatment with OxPAPC induced gene expression of enzymes involved in the PPP, including *Pgd*, *G6pd*, and *Taldo*, in a time- and concentration-dependent manner (Figure 2F).

These data demonstrate that a redox-regulatory metabolism in Mox macrophages is fueled by glucose with a concomitant shift to the PPP to support newly expressed antioxidant genes and GSH production.

3.3. The macrophage metabolic adaptation to OxPLs involves transient suppression of aerobic glycolysis accompanied by Hif1α-dependent and independent gene expression

While homeostatic energy production of resting immune cells is primarily dependent on oxidative phosphorylation, stress conditions and inflammatory stimulation induce a metabolic state that heavily relies on glycolytic bioenergetics [6,48,49]. Phenotypic polarization to pro-inflammatory M1 macrophages involves a switch to Warburg metabolism (aerobic glycolysis) leading to lactate secretion and a succinate-dependent upregulation of inflammatory genes via Hif1α [6]. However, in Mox macrophages, metabolomic analysis showed that intracellular lactate is significantly decreased, strikingly different from LTA-induced M1 macrophages (Figure 3A). Moreover, metabolites of the glycolytic pathway, including fructose-1,6-bisphosphate, dihydroxyacetone phosphate (DHAP), and pyruvate are decreased in Mox, again, strikingly different from LTA-induced M1 and IL4-induced M2 macrophages (Figure 3B). Together, the metabolomic analysis indicated that aerobic glycolysis is suppressed in Mox macrophages. Supporting this notion, extracellular flux analysis of BMDMs and RAW264.7 cells demonstrated that OxPAPC significantly decreased basal and stressed extracellular acidification rate (ECAR), reflecting decreased lactate production (Figure 3C; Figure S2A). Strikingly, treatment with OxPAPC for 4 h inhibited ECAR not only in naïve but also in M1-polarized BMDMs that had been pre-treated with LPS for 16 h (Figure 3D).

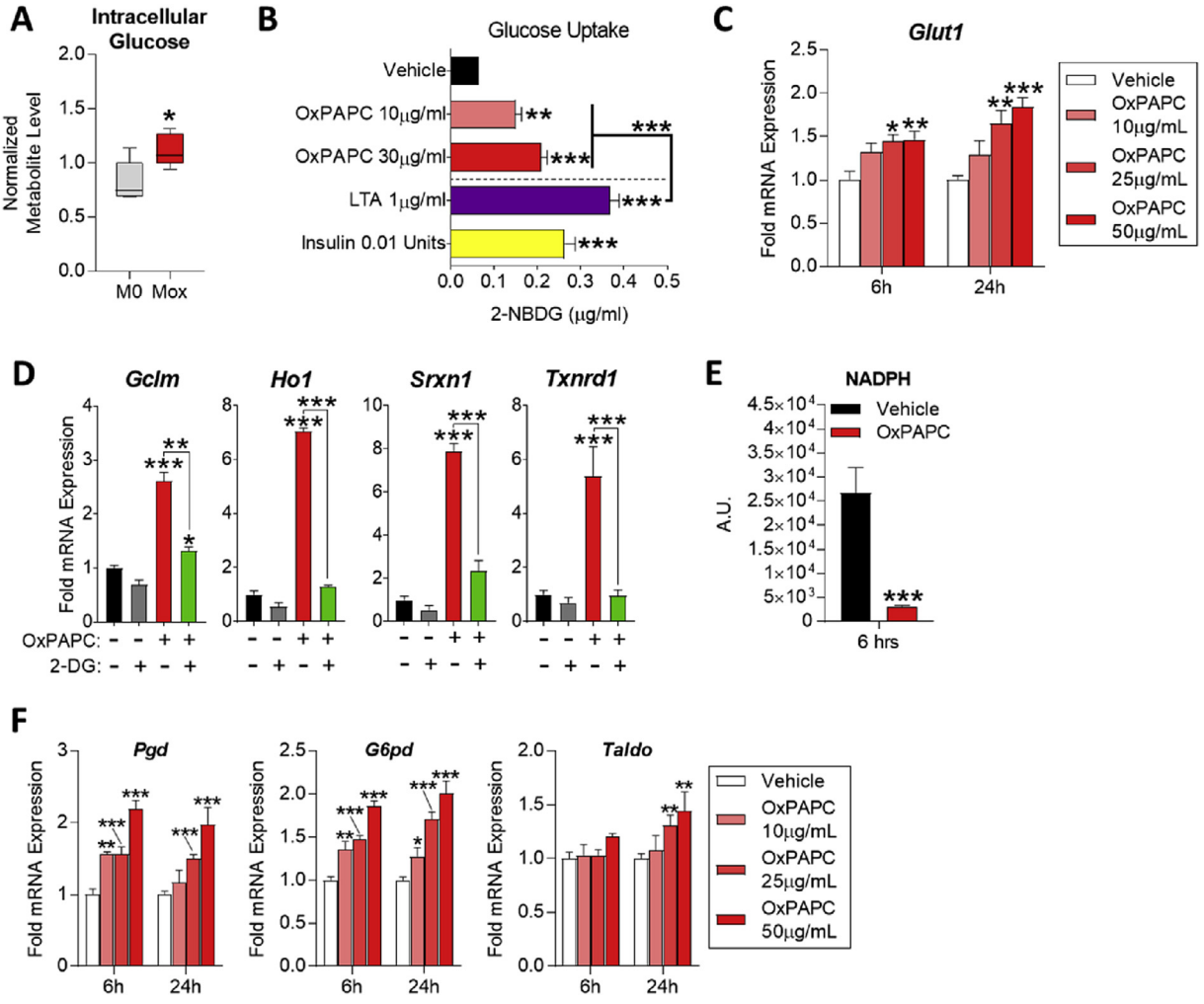

Figure 2: OxPL-treated macrophages induce the pentose phosphate pathway while relying on glucose metabolism for antioxidant gene expression. A. Intracellular glucose levels from metabolomics of polarized BMDMs represented by box and whisker plots (n = 5). **B.** Glucose uptake in BMDMs treated with vehicle (RPMI media), 10–30 μg/mL OxPAPC, 1 μg/mL LTA, or 0.01 units of insulin for 6 h. Uptake measured by fluorescence quantification of 2-NBGD (2-(N-(7-nitrobenz-2-oxa-1,3-diazol-4-yl)amino)-2-deoxy-glucose; fluorescent 2-deoxy-glucose analog) (n = 4). **C.** *Glut1* mRNA expression as measured by qPCR in RAW264.7 cells after 6 and 24 h treatment with vehicle (RPMI media) or 10–50 μg/mL OxPAPC (n = 4). **D.** mRNA expression of redox homeostasis genes measured by qPCR in BMDMs after 4 h treatment with 10 μg/mL OxPAPC and/or 10 mM 2-deoxy-D-glucose (2-DG) (n = 3). **E.** Intracellular NADPH levels in BMDMs treated with 10 μg/mL OxPAPC for 6 h, measured using the NADP/NADPH Assay Kit (Abcam; ab65349) (n = 4). **F.** mRNA expression of pentose phosphate pathway genes measured by qPCR in RAW264.7 cells treated with 10–50 μg/mL OxPAPC for 6 or 24 h. Genes measured include *Pgd*, *G6pdx*, and *Taldo* (n = 4). **G.** mRNA expression of metabolism-related genes measured by qPCR in BMDMs after 24 h treatment with 6.4 μM (50 μg/mL) OxPAPC, OxPAPE, or OxAA (n = 3). Data are expressed as mean ± SEM. Biological replicates indicated by (n). Statistical significance calculated by Welch's 2-sided t-test (*$p \leq 0.05$; **$p < 0.01$; ***$p < 0.001$).

Together, these data point to a novel acute metabolic reprogramming of macrophages in response to OxPLs that is characterized by suppression of aerobic glycolysis.

In M1 macrophages, increased aerobic glycolysis has been linked to inflammatory gene expression including *Il1β*, by a mechanism involving Hif1α [6]. However, using BMDMs isolated from Hif1α-deficient mice [50], we found that OxPAPC-induced *Il1β* expression was independent of Hif1α, while OxPAPC-induced expression of *Glut1* and *Vegf* required Hif1α (Figure 3E). Nevertheless, OxPAPC-induced *Glut1*, *Vegf*, and *Il1β* all were dependent on glycolysis, since inhibition of glucose phosphorylation blocked OxPAPC-induced expression of these genes (Figure 3F). Inhibition of pyruvate transport into mitochondria significantly reduced OxPAPC-induced *Il1β*, while increasing Nrf2-dependent *Ho1* gene expression (Figure S2D), which did not require Hif1α (Figure S2E) and was restricted to early time points (Figure S2F). In contrast, OxPAPC-induced expression of genes involved in glycolysis and the PPP was sustained for up to 24 h (Figure 2C and F), indicating metabolic adaptation of macrophages to these oxidation-derived DAMPs. To further investigate the long-term adaptation of macrophages to OxPLs, we treated BMDMs with OxPAPC for 24 h and then analyzed ECAR to assess aerobic glycolysis. Compared to the vehicle control, long-term exposure of macrophages to OxPAPC significantly increased ECAR in a concentration-dependent manner (Figure 3G). As previously reported, alternatively activated M2 polarization by IL4 for 24 h also increased lactate production [51] and classically activated M1 polarization using LPS & INFγ resulted in the expected strong shift towards aerobic glycolysis (Figure 3G).

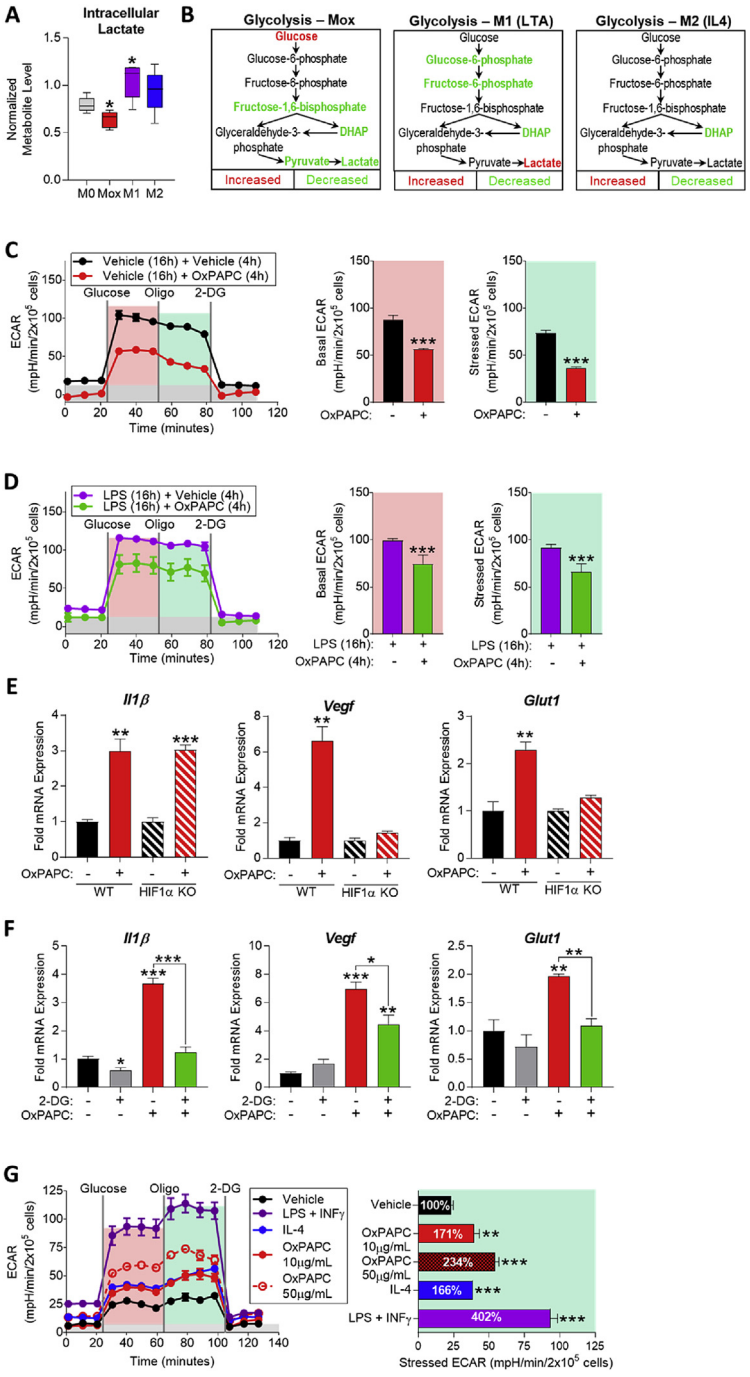

Figure 3: The macrophage metabolic adaptation to OxPLs involves transient suppression of aerobic glycolysis and HIF1α-dependent and independent gene expression. A. Intracellular lactate from metabolomics of M0 (vehicle, RPMI media), Mox (10 μg/mL OxPAPC), M1 (1 μg/mL LTA), and M2 (10 ng/mL IL4) BMDMs (6 h) represented by box and whisker plots (n = 5). **B.** Glycolysis pathway in Mox, M1, and M2 BMDMs (6 h) (n = 5). **C.** Glycolytic stress test (GST) of BMDMs treated with vehicle (RPMI media) or 10 μg/mL OxPAPC for 4 h (n = 4). The extracellular acidification rate (ECAR) was measured after injection of 20 mM glucose, 1 μM oligomycin, and 80 mM 2-DG addition to produce the basal (red), stressed (teal), and background (gray) ECAR, respectively. Basal and stressed ECAR were calculated by subtracting the mean ECAR of the post-glucose (basal) or post-Oligomycin (stressed) measurements from the mean ECAR of the post-2-DG measurements. **D.** GST of BMDMs treated with 1 μg/mL LPS for 16 h to induce M1 polarization, followed by 4 h treatment of vehicle (RPMI media) or 10 μg/mL OxPAPC (n = 4). **E.** mRNA expression of *Il1β*, *Vegf*, and *Glut1* measured by qPCR in WT and HIF1α-KO BMDMs treated with vehicle or 50 μg/mL OxPAPC for 6 h (n = 4). **F.** mRNA expression of *Il1β*, *Vegf*, and *Glut1* measured by qPCR in WT BMDMs treated with 10 mM 2-DG and/or 10 μg/mL OxPAPC for 4 h (n = 3). **G.** GST of BMDMs treated with vehicle, 1 μg/mL LPS (M1), 10 ng/mL IL4 (M2), or 10–50 μg/mL OxPAPC (Mox) for 24 h (n = 4). Data are expressed as mean ± SEM. Biological replicates indicated by (n). Statistical significance calculated by Welch's 2-sided t-test (*$p \leq 0.05$; **$p < 0.01$; ***$p < 0.001$).

Taken together, these data demonstrate that, through suppression of aerobic glycolysis, OxPLs acutely reprogram glucose metabolism in macrophages to support production of NADPH, antioxidant enzymes, and antioxidant metabolites. The results implicate different metabolic requirements for Hif1α and Nrf2-dependent gene expression in Mox macrophages and also raise the possibility that different OxPL species present in OxPAPC selectively induce inflammatory versus metabolic and antioxidant gene expression. Long-term adaptation to OxPLs, once GSH levels return to normal, results in a sustained, elevated use of glucose that may be eventually converted to lactate. Furthermore, the fact that glucose taken up by Mox macrophages is not initially converted to lactate, as in M1 macrophages, implies that it is instead converted to pyruvate, which enters the TCA cycle.

3.4. OxPLs redirect TCA metabolism and inhibit macrophage respiratory capacity

Analysis of TCA cycle metabolites revealed that α-ketoglutarate levels were significantly lower in Mox macrophages, compared to M0, M1, or M2 macrophages (Figure 4A). α-ketoglutarate can be metabolized to glutamate, one of the essential substrates for GSH synthesis [52], by aspartate transaminase (AST or *Got1*) [53]. In support of this mechanism, we have previously shown that *Got1* is significantly upregulated in Mox, but not in M1 or M2 macrophages [9]. These findings indicate that OxPLs impact TCA metabolism. Analyses of mitochondrial gene expression demonstrated significantly lower expression of *Cox5b*, a complex IV component after 4 h of treatment with OxPAPC (Figure S3A). Moreover, we found that succinate levels were significantly increased (Figure 4B), while succinate dehydrogenase (SDH; a component of TCA cycle and electron transport chain) mRNA levels were significantly decreased (Figure 4C) and protein levels trended to be lower in Mox macrophages (Figure S3B). Levels of methylmalonate, an inhibitor of SDH [54], were significantly increased in Mox macrophages (Figure 4D). In addition, we found that levels of a variety of carnitines, molecules essential for β-oxidation through facilitation of mitochondrial fatty acid transport, were significantly decreased in Mox macrophages (Table S1). Together, these data demonstrate that in contrast to M1 and M2 macrophages, Mox macrophages redirect the flux of TCA intermediates towards GSH synthesis at the level of SDH (Figure 4E), indicating a unique glucose utilization mechanism supporting redox homeostasis.

To examine the consequences of this metabolic switch for oxidative phosphorylation (OXPHOS) in Mox macrophages, we treated BMDMs with OxPAPC and measured respiratory capacity by analyzing oxygen consumption rate (OCR). We found that OxPAPC inhibited macrophage respiration after 4 h, demonstrated by a depressed basal and maximal OCR (Figure 4F). OxPAPC also inhibited OCR in RAW264.7 macrophages (Figure S3C). This effect was replicated in BMDMs with OxPAPE, suggesting that this effect is not phospholipid head group dependent (Figure 4G). To test whether the oxidized moiety is the structural component of OxPL responsible for the effects seen, we treated BMDMs with non-enzymatically oxidized arachidonic acid (OxAA) and found that the antioxidant, inflammatory, and metabolic gene expression were induced to the same extent as with OxPAPC and OxPAPE (Figure S3D). This effect was dependent on oxidative modification of the phospholipid, since neither PAPC nor dimystiroylphosphatidylcholine (DMPC, a phospholipid containing saturated fatty acids and thus cannot be oxidized) inhibited respiratory capacity (data not shown). The inhibition of respiratory capacity of LysoPC was not to the same extent as OxPAPC, or POVPC and PGPC, nor did LysoPC inhibit the glycolytic capacity of macrophages (Figure S3E). To test whether the effect of OxPLs on mitochondrial respiration was immediate, we directly injected OxPAPC to the cells during the stress test. While exposure to OxPAPC did not affect basal OCR within the first 2 h, the maximal OCR was significantly inhibited (Figure 4H), indicating that the electron transport chain within mitochondria is affected. M2 polarization with IL4 was shown to increase OCR [7]; however, we found that OxPAPC inhibits respiratory capacity of M2-polarized macrophages, essentially overriding the effect of IL4 (Figure 4I).

3.5. Mitochondrial inhibition by OxPLs requires TLR2-dependent ceramide accumulation

We have previously shown that OxPL-induced inflammatory gene expression is dependent on TLR2 [18]. To test whether TLR2 also mediates inhibition of OCR by OxPLs, we used BMDMs isolated from TLR2 deficient mice, which were resistant to OxPAPC-induced *Cxcl1* expression (Figure 5A). In contrast, OxPAPC-induced *Ho1* expression, which is known to be mediated by Nrf2 [9,18], was independent of TLR2 (Figure 5A). We demonstrate that mitochondrial inhibition by OxPAPC was also attenuated in TLR2-deficient macrophages (Figure 5B), but not in Nrf2-deficient macrophages (Figure 5C).

Ceramides, products of sphingosine and sphingomyelin metabolism, were shown to directly affect cellular metabolism by inhibiting mitochondrial function [55], and it was previously shown that OxPLs induce ceramide accumulation in RAW264.7 macrophages [56]. Using liquid chromatography—mass spectrometry (LC—MS), we demonstrate here that OxPAPC induced significant ceramide accumulation in BMDMs as early as 4 h (Figure S4A). Furthermore, we found that OxPAPC did not induce ceramide accumulation in TLR2-deficient macrophages (Figure 5D).

Further investigation of the mechanism involved in OxPL-induced ceramide production revealed that neither OxPAPC nor its component PGPC significantly affected gene expression of any of the 6 ceramide synthases (*CerS1-6*) (Figure S4B), indicating that activation of enzymatic activity mediates increased ceramide levels. Ceramide synthesis occurs by two pathways: 1) *de novo* ceramide synthesis and 2) sphingomyelin recycling (Figure 5E), which can be assessed using the serine palmitoyltransferase inhibitor myriocin or the neutral sphingomyelinase inhibitor 3-O-methyl-sphingomyelin (3OMS), respectively. We found that inhibition of neutral sphingomyelinase abolished, while inhibition of serine palmitoyltransferase only partially affected the inhibitory effect of OxPAPC on respiratory capacity (Figure 5F; Figure S4C).

Together, these data show that macrophages sense OxPL species via TLR2 to suppress mitochondrial function and OXPHOS, primarily through a neutral sphingomyelin recycling mechanism of ceramide accumulation.

3.6. Spleen tyrosine kinase (Syk) is a key mediator of OxPL-induced inflammatory gene expression, ceramide accumulation, and mitochondrial inhibition

Recently, Syk has been implicated in TLR2 signaling [29—31]. To test if Syk is involved in OxPL-induced inflammatory gene expression and mitochondrial inhibition, we treated wild-type and Syk-KO BMDMs with OxPAPC. We found that inflammatory gene expression was significantly blunted in Syk-KO macrophages, while antioxidant gene expression was not affected (Figure 6A). Furthermore, treatment with the Syk inhibitor piceatannol inhibited OxPAPC-induced inflammatory gene expression (Figure 6B). To test whether inhibition of Syk would affect OxPL-induced ceramide accumulation in macrophages, we used the Syk inhibitor R406 (the active version of the prodrug fostamatinib). We found that R406 ablated OxPAPC-induced ceramide accumulation and restored mitochondrial function in macrophages (Figure 6C and D). Taken together, these data demonstrate that Syk is a crucial mediator

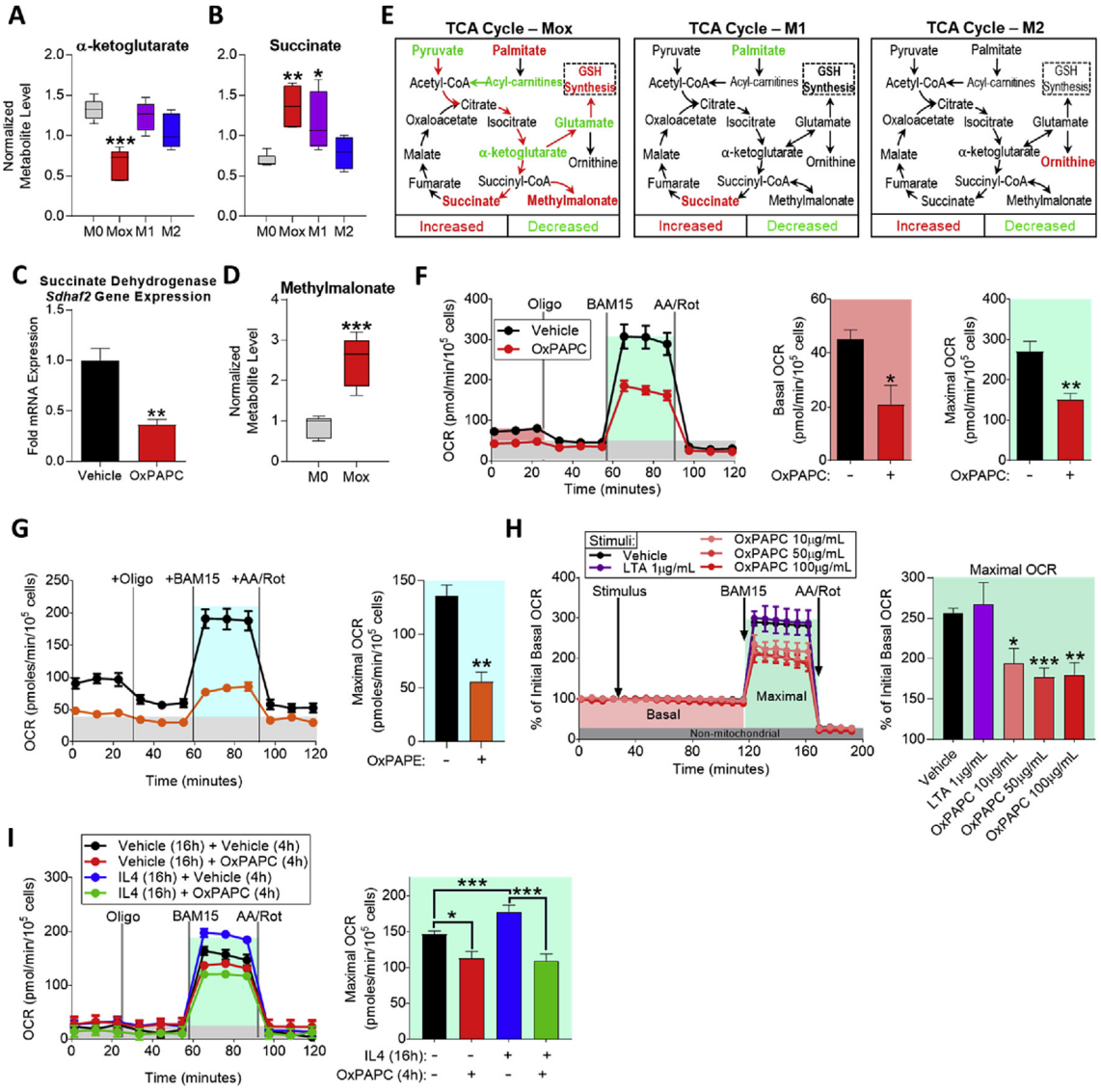

Figure 4: OxPLs redirect TCA metabolism and inhibit macrophage respiratory capacity. A. Intracellular α-ketoglutarate from metabolomics of M0 (vehicle, RPMI media), Mox (10 μg/mL OxPAPC), M1 (1 μg/mL LTA), and M2 (10 ng/mL IL4) BMDMs (6 h) represented by box and whisker plots (n = 5). **B.** Intracellular succinate from metabolomics of M0, Mox, M1, and M2 BMDMs (6 h) represented by box and whisker plots (n = 5). **C.** mRNA expression of nuclear-encoded complex II subunit, *Sdhaf2*, as measured by qPCR in BMDMs treated with vehicle or 10 μg/mL OxPAPC for 4 h (n = 4). **D.** Fold change of intracellular succinate dehydrogenase inhibitor, methylmalonate, in Mox BMDMs compared to M0 as found by metabolomics (n = 5). **E.** The tri-carboxylic acid (TCA) cycle in Mox, M1, and M2 BMDMs, highlighting metabolites significantly changed from M0 (n = 5). **F.** Mitochondrial stress test (MST) of BMDMs treated with vehicle (RPMI media) or 10 μg/mL OxPAPC for 4 h (n = 4). The oxygen consumption rate (OCR) was measured initially (basal; red), and after injection of 1 μM oligomycin, 2 μM of the uncoupler BAM15 (maximal; teal), and 10 μM antimycin A & 1 μM rotenone (AA/Rot; gray; non-mitochondrial). Basal and maximal OCR were calculated by subtracting the mean OCR of the first three (basal) or post-BAM15 (maximal) measurements from the mean OCR of the post-AA/Rot measurements. **G.** MST of BMDMs treated with vehicle (RPMI media) or 30 μg/mL OxPAPE for 4 h (n = 4). **H.** Basal and maximal oxygen consumption rate (OCR) measured in BMDMs treated acutely with vehicle, 1 μg/mL LTA, or 10–100 μg/mL OxPAPC. Treatment was injected into wells containing BMDMs after 30 min of unstimulated measurement. OCR was measured for 2 h (basal) after which 2 μM BAM15 was injected to assess maximal OCR. Antimycin A and rotenone were injected to determine the non-mitochondrial OCR (background). Data represented as %OCR, where 100% refers to the unstimulated basal OCR (n = 4). **I.** MST of BMDMs treated with vehicle (RPMI media) or 10 ng/mL IL4 for 16 h, followed by vehicle (RPMI media) or 10 μg/mL OxPAPC for 4 h (n = 4). Data are expressed as mean ± SEM. Biological replicates indicated by (n). Statistical significance calculated by Welch's 2-sided t-test (*$p \leq 0.05$; **$p < 0.01$; ***$p < 0.001$).

for OxPL-induced cellular signaling and they indicate that Syk inhibition is a viable approach to inhibiting OxPL-driven inflammatory gene expression and mitochondrial inhibition.

4. DISCUSSION & CONCLUSION

Cellular metabolism of immune cells has risen to the forefront of immunology research, with landmark studies showing that classically activated pro-inflammatory macrophages rely on aerobic glycolysis [6], while alternatively activated anti-inflammatory macrophages require oxidative phosphorylation [7]. Here we show for the first time that in response to OxPLs, which are oxidation-derived DAMPs, macrophages reprogram their metabolism to either support redox-regulatory or inflammatory mechanisms. We further identify Syk as a common downstream mediator that is involved in both OxPL-induced ceramide production and inflammatory gene expression.

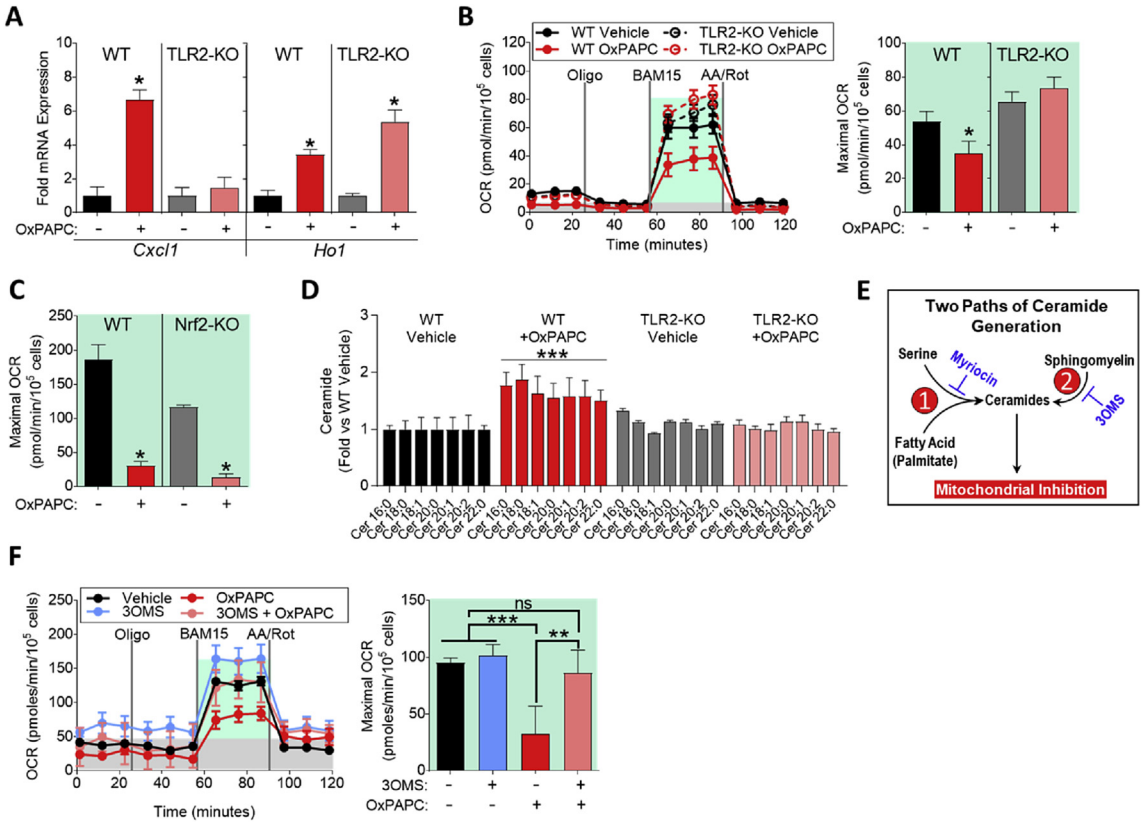

Figure 5: Mitochondrial inhibition by OxPLs requires TLR2-dependent ceramide accumulation. A. mRNA expression of *Cxcl1* and *Ho1* measured by qPCR in WT or TLR2-KO BMDMs treated with vehicle or 10 μg/mL OxPAPC for 4 h (n = 3). **B.** MST of WT or TLR2-KO BMDMs treated with vehicle or 10 μg/mL OxPAPC for 4 h (n = 4). **C.** Maximal OCR calculated from the MST of WT (C57BL/6) or Nrf2-KO BMDMs treated with 10 μg/mL OxPAPC for 4 h (n = 4). **D.** Fold change in ceramide accumulation as measured by liquid chromatography—mass spectrometry (LC—MS) of WT or TLR2-KO BMDMs treated with vehicle or 30 μg/mL OxPAPC for 16 h (n = 5). Ceramides were quantified on an individual species basis, using the integrated peak area of the ion count. The integrated peak area of each analyte was normalized to the internal standard, Cer17:0, and to the protein content of each sample as determined by a Bradford assay. Significance was determined by two-way ANOVA of the ion count peak area. Data represented in as fold change compared to WT vehicle control. **E.** Summary of two pathways leading to ceramide generation in cells. Pathway 1, referred to as *de novo* ceramide biogenesis, contains the rate-limiting enzyme serine-palmitoyl-transferase 1, which is inhibited by myriocin. Pathway 2, referred to as sphingomyelin recycling, contains acidic and neutral sphingomyelinases as the rate-limiting enzymes. 3-O-methyl-sphingomyelin (3OMS) inhibits neutral sphingomyelinase. **F.** MST of WT BMDMs treated with 10 μg/mL OxPAPC and/or 1 μM 3-O-methyl-sphingomyelin (3OMS), an inhibitor of neutral sphingomyelinase, for 4 h (n = 4). Data are expressed as mean ± SEM. Biological replicates indicated by (n). Statistical significance calculated by Welch's 2-sided t-test ($*p \leq 0.05$; $**p < 0.01$; $***p < 0.001$).

We find that OxPLs drive production of glutathione in macrophages in a glucose-dependent manner. The production of glutathione, supported by Nrf2-dependent enzyme expression, is unique to Mox macrophages when compared to M1 and M2 macrophages. OxPLs initially deplete glutathione as well as NADPH in macrophages, but glutathione is eventually replenished through a mechanism requiring functional glucose metabolism. This effect is not regulated by TLR2 stimulation alone, as macrophages did not produce glutathione upon stimulation with the TLR2 ligand LTA.

Furthermore, we show that PPP enzymes are upregulated and sustained after OxPAPC treatment, providing a source of NADPH necessary to produce glutathione and the function of Nrf2-dependent antioxidant enzymes. The switch to aerobic glycolysis (referred to as the Warburg effect) has been shown to be necessary for pro-inflammatory cytokine production by M1 macrophages [6]. In contrast, OxPAPC acutely inhibits lactate production in both naïve (M0) and already glycolytic (M1 and RAW264.7) macrophages. Surprisingly, Mox macrophages still upregulate pro-inflammatory gene expression, and we have shown that they secrete IL1β [18]. We find that OxPAPC induces expression of the glucose transporter *Glut1* via Hif1α, and that Mox macrophages indeed have increased glucose uptake.

After long-term exposure to OxPAPC (24 h), Mox macrophages switch to lactate production. Concurrently, long-term exposure of macrophages to OxPAPC leads to the restoration of glutathione levels and the abrogation of Nrf2-dependent gene expression while the glucose uptake and PPP-related gene expression remains sustained, indicating an increased potential for glucose metabolism. The two main fates of the glucose-derived metabolite pyruvate are to be converted to lactate or to be transported to the mitochondria for use in the TCA cycle. OxPAPC-treated cells do not acutely promote pyruvate conversion to lactate, given the dramatic decrease we see in ECAR. Instead, our data are consistent with pyruvate being shuttled to the mitochondria for further processing. A striking observation was that Mox macrophages have significantly lower levels of α-ketoglutarate (a Hif1α-repressor [57] and component of the TCA cycle), while having significantly increased levels of succinate (a Hif1α-stabilizer) [57,58], which may explain how metabolism in Mox macrophages is linked to Hif1α-dependent gene expression.

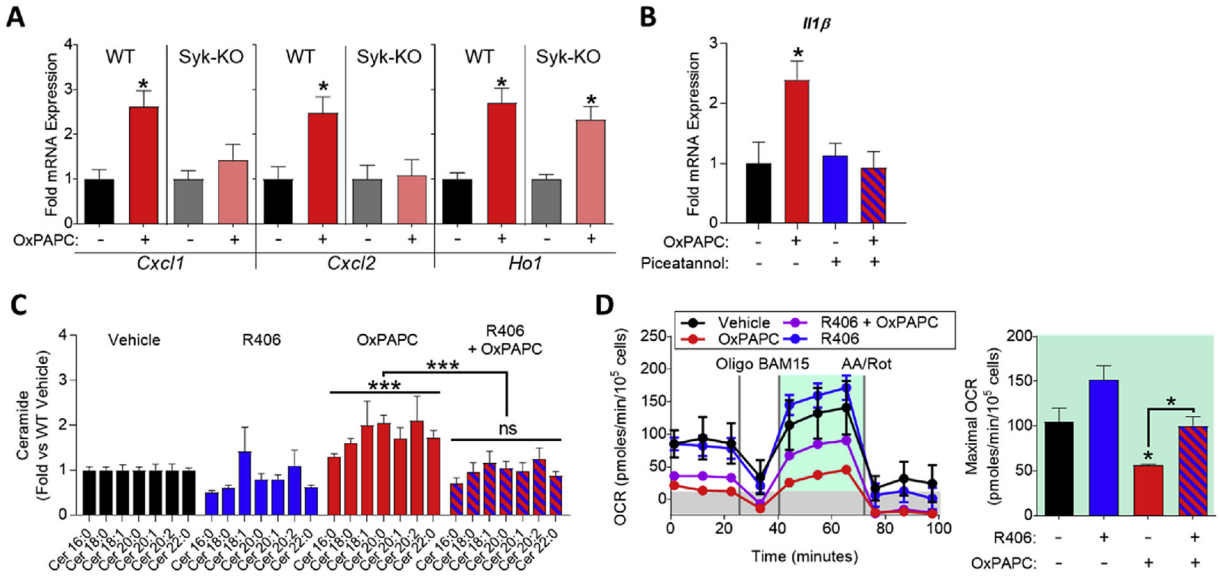

Figure 6: Spleen tyrosine kinase (Syk) is a key mediator of OxPL-induced inflammatory gene expression, ceramide accumulation, and mitochondrial inhibition. A. mRNA expression of *Cxcl1*, *Cxcl2*, and *Ho1* measured by qPCR in WT or Syk-KO BMDMs treated with vehicle or 10 μg/mL OxPAPC for 4 h (n = 3). **B.** mRNA expression of *Il1* measured by qPCR in RAW264.7 macrophages treated with vehicle or 10 μg/mL OxPAPC for 4 h (n = 3). **C.** Fold change in ceramide accumulation as measured by liquid chromatography−mass spectrometry (LC−MS) of BMDMs treated with vehicle or 30 μg/mL OxPAPC or 50 nM R406 (Syk inhibitor) for 16 h (n ≥ 4). Ceramides were quantified on an individual species basis, using the integrated peak area of the ion count. The integrated peak area of each analyte was normalized to the internal standard, Cer17:0, and to the protein content of each sample as determined by a Bradford assay. Significance was determined by two-way ANOVA of the ion count peak area. Data represented in as fold change compared to vehicle control. **D.** MST of BMDMs treated with 10 μg/mL OxPAPC and/or 5 μM R406 for 4 h (n = 4). Data are expressed as mean ± SEM. Biological replicates indicated by (n). Statistical significance calculated by Welch's 2-sided t-test (*$p \leq 0.05$; **$p < 0.01$; ***$p < 0.001$).

It has previously been reported that OxPLs induce ceramide accumulation in macrophages [56,59]. Here we find that OxPAPC induced ceramide accumulation in macrophages by a mechanism involving TLR2. Inhibition of mainly sphingomyelin recycling, but also inhibition of *de novo* ceramide synthesis, abrogated OxPAPC-induced mitochondrial inhibition. Ceramide accumulation has been linked to mitochondrial dysfunction, and we find that macrophages deficient in TLR2, but not Nrf2, were protected against OxPAPC-induced mitochondrial dysfunction.

Finally, we identify Syk as a key mediator of OxPL-induced effects that are downstream of TLR2. Genetic deletion or pharmacologic inhibition of Syk abrogated OxPL-induced inflammatory gene expression, ceramide accumulation, and mitochondrial inhibition, without inhibiting antioxidant gene expression. Syk inhibitors are being tested in preclinical and clinical studies for the treatment of chronic inflammatory disorders [28,60,61], and, based on our findings, Syk may be a viable therapeutic target to inhibit the perceived negative effects of OxPL in the context of cardiometabolic diseases as well.

Taken together, we show that OxPLs, through a TLR2 and Syk-driven mechanism, reprogram macrophage metabolism, which together with Nrf2-dependent gene expression, is required for production of antioxidant metabolites. In addition, we discovered that metabolic changes in Mox macrophages are tightly linked to redox-regulatory and inflammatory gene expression. Our study provides novel insight into the immunometabolic mechanisms that regulate the translation of oxidative tissue damage into chronic inflammatory responses.

AUTHOR CONTRIBUTIONS

Conceptualization, V.S. and N.L.; Methodology, V.S., K.W.A., D.D., and C.U.; Validation, V.S., C.U., P.V., D.D.; Formal Analysis, V.S., C.U., P.V., D.D., and G.B.; Investigation, V.S., K.W.A., C.U., G.B., P.V., D.D., and A.K.M.; Writing — Original Draft, V.S. and N.L.; Writing — Review & Editing, V.S. and N.L.; Visualization, V.S., C.U., and N.L.; Funding Acquisition, V.S. and N.L.; Resources, N.L., T.E.H.; Project Administration, V.S. and N.L.; Supervision, N.L.

ACKNOWLEDGMENTS

This work was supported by NIH grants R01 DK096076 (to N.L.), P01 HL120840 (to N.L.), and UVA Double-Hoo Research Award (to V.S. and D.D.). V.S. was supported by pre-doctoral fellowships from NIH (5 F31 DK108553-02), AHA (15 PRE 255600036), Pharmacological Sciences Training Grant (5 T32 GM007055-40), and an SFRBM Mini-fellowship. C.U. was supported by the Pharmacological Sciences Training Grant (5 T32 GM007055-43). A.K.M. was supported by National Scientist Development Grant (14SDG20380044 to A.K.M.).

CONFLICT OF INTEREST

None declared.

APPENDIX A. SUPPLEMENTARY DATA

Supplementary data related to this article can be found at https://doi.org/10.1016/j.molmet.2017.11.002.

REFERENCES

[1] Okabe, Y., Medzhitov, R., 2015. Tissue biology perspective on macrophages. Nature Immunology 17(1):9—17. https://doi.org/10.1038/ni.3320.

[2] Davies, L.C., Jenkins, S.J., Allen, J.E., Taylor, P.R., 2013. Tissue-resident macrophages. Nature Immunology 14(10):986—995. https://doi.org/10.1038/ni.2705.

[3] Stienstra, R., Netea-Maier, R.T., Riksen, N.P., Joosten, L.A.B., Netea, M.G., 2017. Specific and complex reprogramming of cellular metabolism in myeloid cells during innate immune responses. Cell Metabolism 26(1):142—156. https://doi.org/10.1016/j.cmet.2017.06.001.

[4] Cheng, S.-C., Scicluna, B.P., Arts, R.J.W., Gresnigt, M.S., Lachmandas, E., Giamarellos-Bourboulis, E.J., et al., 2016. Broad defects in the energy metabolism of leukocytes underlie immunoparalysis in sepsis. Nature Immunology (January). https://doi.org/10.1038/ni.3398.

[5] Norata, G.D.D., Caligiuri, G., Chavakis, T., Matarese, G., Netea, M.G.G., Nicoletti, A., et al., 2015. The cellular and molecular basis of translational immunometabolism. Immunity 43(3):421—434. https://doi.org/10.1016/j.immuni.2015.08.023.

[6] Tannahill, G.M., Curtis, A.M., Adamik, J., Palsson-McDermott, E.M., McGettrick, A.F., Goel, G., et al., 2013. Succinate is an inflammatory signal that induces IL-1β through HIF-1α. Nature 496(7444):238—242 https://doi.org/10.1038/nature11986.

[7] Huang, S.C., Everts, B., Ivanova, Y., Sullivan, D.O., Nascimento, M., Smith, A.M., et al., 2014. Cell-intrinsic lysosomal lipolysis is essential for alternative activation of macrophages. Nature Immunology 15(August):1—12. https://doi.org/10.1038/ni.2956.

[8] Jha, A.K., Huang, S.C.-C.C., Sergushichev, A., Lampropoulou, V., Ivanova, Y., Loginicheva, E., et al., 2015. Network integration of parallel metabolic and transcriptional data reveals metabolic modules that regulate macrophage polarization. Immunity 42(3):419—430. https://doi.org/10.1016/j.immuni.2015.02.005.

[9] Kadl, A., Meher, A.K., Sharma, P.R.P.P.R., Lee, M.Y., Doran, A.C., Johnstone, S.R., et al., 2010. Identification of a novel macrophage phenotype that develops in response to atherogenic phospholipids via Nrf2. Circulation Research 107(6):737—746. https://doi.org/10.1161/CIRCRESAHA.109.215715.

[10] Kamstrup, P.R., Hung, M.-Y., Witztum, J.L., Tsimikas, S., Nordestgaard, B.G., 2017. Oxidized phospholipids and risk of calcific aortic valve disease. Arteriosclerosis, Thrombosis, and Vascular Biology. https://doi.org/10.1161/ATVBAHA.116.308761.

[11] Capoulade, R., Chan, K.L., Yeang, C., Mathieu, P., Bossé, Y., Dumesnil, J.G., et al., 2015. Oxidized phospholipids, lipoprotein(a), and progression of calcific aortic valve stenosis. Journal of the American College of Cardiology 66(11):1236—1246. https://doi.org/10.1016/j.jacc.2015.07.020.

[12] Tsimikas, S., Witztum, J.L., 2008. The role of oxidized phospholipids in mediating lipoprotein(a) atherogenicity. Current Opinion in Lipidology 19(4):369—377. https://doi.org/10.1097/MOL.0b013e328308b622.

[13] Tsimikas, S., Bergmark, C., Beyer, R.W., Patel, R., Pattison, J., Miller, E., et al., 2003. Temporal increases in plasma markers of oxidized low-density lipoprotein strongly reflect the presence of acute coronary syndromes. Journal of the American College of Cardiology 41(3):360—370. https://doi.org/10.1016/S0735-1097(02)02769-9.

[14] Watson, a D., Leitinger, N., Navab, M., Faull, K.F., Hörkkö, S., Witztum, J.L., et al., 1997. Structural identification by mass spectrometry of oxidized phospholipids in minimally oxidized low density lipoprotein that induce monocyte/endothelial interactions and evidence for their presence in vivo. The Journal of Biological Chemistry 272(21):13597—13607.

[15] Berliner, J.A., Leitinger, N., Tsimikas, S., 2009. The role of oxidized phospholipids in atherosclerosis. Journal of Lipid Research 50(Suppl):S207—S212. https://doi.org/10.1194/jlr.R800074-JLR200.

[16] Leitinger, N., Watson, A.D., Faull, K.F., Fogelman, A.M., Berliner, J.A., 1997. Monocyte binding to endothelial cells induced by oxidized phospholipids present in minimally oxidized low density lipoprotein is inhibited by a platelet activating factor receptor antagonist. Advances in Experimental Medicine and Biology 433:379—382.

[17] Miller, Y.I., Shyy, J.Y.-J., 2016. Context-dependent role of oxidized lipids and lipoproteins in inflammation. Trends in Endocrinology & Metabolism, 1—10. https://doi.org/10.1016/j.tem.2016.11.002.

[18] Kadl, A., Sharma, P.R.P.P.R., Chen, W., Agrawal, R., Meher, A.K., Rudraiah, S., et al., 2011. Oxidized phospholipid-induced inflammation is mediated by Toll-like receptor 2. Free Radical Biology & Medicine 51(10):1903—1909. https://doi.org/10.1016/j.freeradbiomed.2011.08.026.

[19] Serbulea, V., DeWeese, D., Leitinger, N., 2017. The effect of oxidized phospholipids on phenotypic polarization and function of macrophages. Free Radical Biology & Medicine(December 2016):0—1. https://doi.org/10.1016/j.freeradbiomed.2017.02.035.

[20] Mauerhofer, C., Philippova, M., Oskolkova, O.V., Bochkov, V.N., 2016. Hormetic and anti-inflammatory properties of oxidized phospholipids. Molecular Aspects of Medicine 49(July):78—90. https://doi.org/10.1016/j.mam.2016.02.003.

[21] Friedli, O., Freigang, S., 2017. Cyclopentenone-containing oxidized phospholipids and their isoprostanes as pro-resolving mediators of inflammation. Biochimica et Biophysica Acta — Molecular and Cell Biology of Lipids 1862(4):382—392. https://doi.org/10.1016/j.bbalip.2016.07.006.

[22] Egger, J., Bretscher, P., Freigang, S., Kopf, M., Carreira, E.M., 2014. Discovery of a highly potent anti-inflammatory epoxyisoprostane-derived lactone: 2—5.

[23] Bretscher, P., Egger, J., Shamshiev, A., Trötzmüller, M., Köfeler, H., Carreira, E.M., et al., 2015. Phospholipid oxidation generates potent anti-inflammatory lipid mediators that mimic structurally related pro-resolving eicosanoids by activating Nrf 2. EMBO Molecular Medicine 7(5):1—16. https://doi.org/10.15252/emmm.201404702.

[24] Von Schlieffen, E., Oskolkova, O.V., Schabbauer, G., Gruber, F., Blüml, S., Genest, M., et al., 2009. Multi-hit inhibition of circulating and cell-associated components of the toll-like receptor 4 pathway by oxidized phospholipids. Arteriosclerosis, Thrombosis, and Vascular Biology 29(3):356—362. https://doi.org/10.1161/ATVBAHA.108.173799.

[25] Bochkov, V., Kadl, A., Huber, J., Gruber, F., Binder, B.R., Leitinger, N., 2002. Protective role of phospholipid oxidation products in endotoxin-induced tissue damage. Nature 4(June):77—81. https://doi.org/10.1038/nature00954.1.

[26] Zanoni, I., Tan, Y., Di Gioia, M., Broggi, A., Ruan, J., Shi, J., et al., 2016. An endogenous caspase-11 ligand elicits interleukin-1 release from living dendritic cells. Science 352(6290):1—9. https://doi.org/10.1126/science.aaf3036.

[27] Bochkov, V.N., Oskolkova, O.V., Birukov, K.G., Levonen, A.-L., Binder, C.J., Stöckl, J., 2010. Generation and biological activities of oxidized phospholipids. Antioxidants & Redox Signaling 12(8):1009—1059. https://doi.org/10.1089/ars.2009.2597.

[28] Mcadoo, S.P., Tam, F.W.K., 2009. Fostamatinib disodium. Drug Data Report 31(2):173. https://doi.org/10.1358/ddr.2009.031.02.1299360.

[29] Dennehy, K.M., Ferwerda, G., Faro-Trindade, I., Pyz, E., Willment, J.A., Taylor, P.R., et al., 2008. Syk kinase is required for collaborative cytokine production induced through Dectin-1 and Toll-like receptors. European Journal of Immunology 38(2):500—506. https://doi.org/10.1002/eji.200737741.

[30] Fälker, K., Klarström-Engström, K., Bengtsson, T., Lindahl, T.L., Grenegård, M., 2014. The toll-like receptor 2/1 (TLR2/1) complex initiates human platelet activation via the src/Syk/LAT/PLCγ2 signalling cascade. Cellular Signalling 26(2):279—286. https://doi.org/10.1016/j.cellsig.2013.11.011.

[31] Slack, E.C., Robinson, M.J., Hernanz-Falcón, P., Brown, G.D., Williams, D.L., Schweighoffer, E., et al., 2007. Syk-dependent ERK activation regulates IL-2 and IL-10 production by DC stimulated with zymosan. European Journal of Immunology 37(6):1600—1612. https://doi.org/10.1002/eji.200636830.

[32] van Bergenhenegouwen, J., Plantinga, T.S., Joosten, L.A.B., Netea, M.G., Folkerts, G., Kraneveld, A.D., et al., 2013. TLR2 & Co: a critical analysis of the complex interactions between TLR2 and coreceptors. Journal of Leukocyte Biology 94(5):885—902. https://doi.org/10.1189/jlb.0113003.

[33] Lin, Y.-C., Huang, D.-Y., Chu, C.-L., Lin, Y.-L., Lin, W.-W., 2013. The tyrosine kinase Syk differentially regulates Toll-like receptor signaling downstream of the adaptor molecules TRAF6 and TRAF3. Science Signaling 6(289):ra71. https://doi.org/10.1126/scisignal.2003973.

[34] Choi, S.-H., Harkewicz, R., Lee, J.H., Boullier, A., Almazan, F., Li, A.C., et al., 2009. Lipoprotein accumulation in macrophages via toll-like receptor-4-dependent fluid phase uptake. Circulation Research 104(12):1355—1363. https://doi.org/10.1161/CIRCRESAHA.108.192880.

[35] Bae, Y.S., Lee, J.H., Choi, S.H., Kim, S., Almazan, F., Witztum, J.L., et al., 2009. Macrophages generate reactive oxygen species in response to minimally oxidized low-density lipoprotein: toll-like receptor 4- and spleen tyrosine kinase-dependent activation of NADPH oxidase 2. Circulation Research 104(2): 210—218. https://doi.org/10.1161/CIRCRESAHA.108.181040.

[36] Miller, Y., Choi, S., 2012. The SYK side of TLR4: signalling mechanisms in response to LPS and minimally oxidized LDL. British Journal of Pharmacology 167(5):990—999. https://doi.org/10.1111/j.1476-5381.2012.02097.x.

[37] Hilgendorf, I., Eisele, S., Remer, I., Schmitz, J., Zeschky, K., Colberg, C., et al., 2011. The oral spleen tyrosine kinase inhibitor fostamatinib attenuates inflammation and atherogenesis in low-density lipoprotein receptor-deficient mice. Arteriosclerosis, Thrombosis, and Vascular Biology 31(9):1991—1999. https://doi.org/10.1161/ATVBAHA.111.230847.

[38] Kenwood, B.M., Weaver, J.L., Bajwa, A., Poon, I.K., Byrne, F.L., Murrow, B.A., et al., 2014. Identification of a novel mitochondrial uncoupler that does not depolarize the plasma membrane. Molecular Metabolism 3(2):114—123. https://doi.org/10.1016/j.molmet.2013.11.005.

[39] Van den Bossche, J., Baardman, J., Otto, N.A.A., van der Velden, S., Neele, A.E.E., van den Berg, S.M., et al., 2016. Mitochondrial dysfunction prevents repolarization of inflammatory macrophages. Cell Reports 17(3): 684—696. https://doi.org/10.1016/j.celrep.2016.09.008.

[40] Darley-Usmar, V.M., Severn, A., O'Leary, V.J., Rogers, M., 1991. Treatment of macrophages with oxidized low-density lipoprotein increases their intracellular glutathione content. The Biochemical Journal 278(Pt 2):429—434.

[41] Hayes, J.D., Dinkova-Kostova, A.T., 2014. The Nrf2 regulatory network provides an interface between redox and intermediary metabolism. Trends in Biochemical Sciences 39(4):199—218. https://doi.org/10.1016/j.tibs.2014.02.002.

[42] Holmström, K.M., Baird, L., Zhang, Y., Hargreaves, I., Chalasani, A., Land, J.M., et al., 2013. Nrf2 impacts cellular bioenergetics by controlling substrate availability for mitochondrial respiration. Biology Open 2(8):761—770. https://doi.org/10.1242/bio.20134853.

[43] Cheng, X., Siow, R.C.M.R., Mann, G.E.G., 2011. Impaired Redox signaling and antioxidant gene expression in endothelial cells in diabetes: a role for mitochondria and the nuclear factor-E2-related factor 2-Kelch-like ECH-associated protein 1 defense pathway. Antioxidants & Redox Signaling 14(3):469—487. https://doi.org/10.1089/ars.2010.3283.

[44] Calkins, M., Johnson, D., 2009. The Nrf2/ARE pathway as a potential therapeutic target in neurodegenerative disease. Antioxidants & Redox Signaling 11(3). https://doi.org/10.1089/ars.2008.2242.

[45] Mitsuishi, Y., Taguchi, K., Kawatani, Y., Shibata, T., Nukiwa, T., Aburatani, H., et al., 2012. Nrf2 redirects glucose and glutamine into anabolic pathways in metabolic reprogramming. Cancer Cell 22(1):66—79. https://doi.org/10.1016/j.ccr.2012.05.016.

[46] Freemerman, A.J., Johnson, A.R., Sacks, G.N., Milner, J.J., Kirk, E.L., Troester, M.A., et al., 2014. Metabolic reprogramming of macrophages: glucose transporter 1 (GLUT1)-mediated glucose metabolism drives a proinflammatory phenotype. Journal of Biological Chemistry 289(11):7884—7896. https://doi.org/10.1074/jbc.M113.522037.

[47] Sun, Y., 1990. Free radicals, antioxidant enzymes, and carcinogenesis. Free Radical Biology & Medicine 8(6):583—599. https://doi.org/10.1016/0891-5849(90)90156-D.

[48] Peng, M., Peng, M., Yin, N., Chhangawala, S., Xu, K., Leslie, C.S., et al., 2016. Aerobic glycolysis promotes T helper 1 cell differentiation through an epigenetic mechanism. Science 354(6311):481—484.

[49] Everts, B., Amiel, E., van der Windt, G.J.W., Freitas, T.C., Chott, R., Yarasheski, K.E., et al., 2012. Commitment to glycolysis sustains survival of nitric oxide-producing inflammatory dendritic cells. Blood. https://doi.org/10.1182/blood-2012-03-419747.

[50] Polotsky, V.Y., Savransky, V., Bevans-Fonti, S., Reinke, C., Li, J., Grigoryev, D.N., et al., 2010. Intermittent and sustained hypoxia induce a similar gene expression profile in human aortic endothelial cells. Physiological Genomics 41(3):306—314. https://doi.org/10.1152/physiolgenomics.00091.2009.

[51] Huang, S.C.C., Smith, A.M., Everts, B., Colonna, M., Pearce, E.J., Schilling, J.D., et al., 2016. Metabolic reprogramming mediated by the mTORC2-IRF4 signaling axis is essential for macrophage alternative activation. Immunity 45(4):817—830. https://doi.org/10.1016/j.immuni.2016.09.016.

[52] Lu, S.C., Shelly, C., Lu, M.D., 2014. Glutathione synthesis. Biochimica et Biophysica Acta 1830(5):3143—3153. https://doi.org/10.1016/j.bbagen.2012.09.008.GLUTATHIONE.

[53] Ellinger, J.J., Lewis, I.A., Markley, J.L., 2011. Role of aminotransferases in glutamate metabolism of human erythrocytes. Journal of Biomolecular NMR 49(3—4):221—229. https://doi.org/10.1007/s10858-011-9481-9.

[54] Melo, D.R., Mirandola, S.R., Assunção, N.A., Castilho, R.F., 2012. Methylmalonate impairs mitochondrial respiration supported by NADH-linked substrates: involvement of mitochondrial glutamate metabolism. Journal of Neuroscience Research 90(6):1190—1199. https://doi.org/10.1002/jnr.23020.

[55] Sentelle, R., Senkal, C., Jiang, W., Ponnusamy, S., Gencer, S., Selvam, S., et al., 2012. Ceramide targets autophagosomes to mitochondria and induces lethal mitophagy. Nature Chemical Biology 8(10):831—838. https://doi.org/10.1038/nchembio.1059.Ceramide.

[56] Halasiddappa, L.M., Koefeler, H., Futerman, A.H., Hermetter, A., 2013. Oxidized phospholipids induce ceramide accumulation in RAW 264.7 macrophages: role of ceramide synthases. PLoS One 8(7):e70002. https://doi.org/10.1371/journal.pone.0070002.

[57] MacKenzie, E.D., Selak, M.A., Tennant, D.A., Payne, L.J., Crosby, S., Frederiksen, C.M., et al., 2007. Cell-permeating-ketoglutarate derivatives alleviate pseudohypoxia in succinate dehydrogenase-deficient cells. Molecular and Cellular Biology 27(9):3282—3289. https://doi.org/10.1128/MCB.01927-06.

[58] Gorres, K.L., Raines, R.T., 2010. Prolyl 4-hydroxylase 45.

[59] Walton, K., Gugiu, B., Thomas, M., 2006. A role for neutral sphingomyelinase activation in the inhibition of LPS action by phospholipid oxidation products. Journal of Lipid Research 47(9):1967—1974. https://doi.org/10.1194/jlr.M600060-JLR200.

[60] Weinblatt, M.E., Genovese, M.C., Ho, M., Hollis, S., Rosiak-Jedrychowicz, K., Kavanaugh, A., et al., 2014. Effects of fostamatinib, an oral spleen tyrosine kinase inhibitor, in rheumatoid arthritis patients with an inadequate response to methotrexate: results from a phase iii, multicenter, randomized, double-blind, placebo-controlled, parallel-group study. Arthritis and Rheumatology 66(12):3255—3264. https://doi.org/10.1002/art.38851.

[61] Rolf, M.G., Curwen, J.O., Veldman-jones, M., Eberlein, C., Wang, J., Hellawell, C.J., et al., 2015. In vitro pharmacological profiling of R406 identifies molecular targets underlying the clinical effects of fostamatinib 3:1—12. https://doi.org/10.1002/prp2.175.

